Springer

KSME

Journal of Mechanical Science and Technology 31 (7) (2017) 3465~3473
www.springerlink.com/content/1738-494x(Print)/1976-3824(Online)
DOI 10.1007/s12206-017-0635-x

Development of a two-frequency, elliptical-vibration texturing device for surface texturing †

Rendi Kurniawan[1], Tae Jo Ko[1,*], Li Chang Ping[1], S. Thirumalai Kumaran[1], Gandjar Kiswanto[2], Ping Guo[3] and Kornel F. Ehmann[4]

[1]*School of Mechanical Engineering, Yeungnam University, 214-1, Dae-dong, Gyeongsan-si, Gyeongsangbuk-do 712-749, Korea*
[2]*School of Mechanical Engineering, Universitas Indonesia, 214-1, Kampus Baru UI, Depok 16424, Indonesia*
[3]*Mechanical and Automation Engineering, Chinese University of Hong Kong, Hongkong, China*
[4]*Department of Mechanical Engineering, Northwestern University, 2145 Sheridan Road, Room A215, Evanston, IL 60208, USA*

(Manuscript Received January 13, 2017; Revised March 3, 2017; Accepted March 8, 2017)

Abstract

This study presents the design of a Two-frequency, elliptical-vibration texturing (TFEVT) device. The device was designed to be used in a surface texturing process, and its functionality is based on a combination of ultrasonic (> 20 kHz) and low vibration frequencies (< 100 Hz). The device consists of two parts: The Ultrasonic elliptical motion transducer (UEMT) and the Low frequency displacement amplifier (LFDA). A modal analysis simulation and dynamic experiments were conducted to investigate the dynamic characteristics of the device. The modal simulation was carried out using finite element analysis and the dynamic experiment was evaluated using Frequency response function (FRF) analysis. The working principle of the UEMT is based on a resonance transducer, and the angle between the two Langevin transducers was set as 90°. The UEMT has two vibration modes, symmetric and asymmetric, and according to experimental data, its working frequency is 24 kHz at the 6th resonance vibration mode when a Polycrystalline diamond (PCD) tool is attached. The UEMT is able to generate an elliptical locus that has a vertical amplitude of 1.4 μm and a horizontal amplitude of 0.6 μm, under a phase-shift of 90°. The design of the LFDA is based on a double parallel four-bar flexure hinge, and the displacement output ratio is set to 5. The working principle of the LFDA is based on a non-resonance transducer. The working frequency of the LFDA is below its first of natural frequencies (≈1060 Hz), and it is able to generate sinusoidal motion with a maximum peak-to-peak amplitude of 9 μm. Finally, to investigate the feasibility of the TFEVT device for use in a surface texturing process, several micro-groove cutting tests were performed on an AISI 1045 alloy steel.

Keywords: Modal analysis; Frequency; Ultrasonic; Transducer; Piezo actuator; Surface texturing

1. Introduction

In this study, the development of a Two-frequency, elliptical-vibration texturing (TFEVT) device is proposed for use in a surface texturing process. The TFEVT method incorporates Ultrasonic elliptical-vibration cutting (UEVC) into a Conventional texturing (CT) method. In the CT method [1, 2], a single frequency of sinusoidal motion is generated in the tool tip along the direction of the depth of the cut, creating relative motion between the tool tip and the workpiece surface; this results in the formation of a micro-dimple. The UEVC method is widely known among researchers as a promising cutting method, especially for hard materials ($H_RC > 39$) [3], and the method excels at reducing cutting forces [4], improving surface roughness [5], increasing tool life [6], and suppressing side burrs [7] of micro-grooves. The principle of UEVC [8] is that it creates elliptical motion in the tool tip, which adds secondary motion in the direction of the cut depth, into one-directional vibration cutting (1D-VC). Fundamentally, the TFEVT method combines both methods (UEVC and CT), and the tool tip motion in the TFEVT method can be drawn as shown in Fig. 1.

For instance, the relative motion of the tool tip in the TFEVT method can be expressed as follows:

$$x(t) = a \cdot \cos(2\pi f_h \cdot t + \phi) + V_f \cdot t \quad (1)$$

$$y(t) = b \cdot \cos(2\pi f_h \cdot t) + B \cdot \cos(2\pi f_l \cdot t) \quad (2)$$

where $x(t)$ and $y(t)$ are the tool positions on the x-y plane in the Cartesian coordinate system, f_h is the ultrasonic frequency of the elliptical tool motion (> 20 kHz), f_l is the low vibration frequency of the sinusoidal wave, ϕ is the phase shift, V_f is

*Corresponding author. Tel.: +82 53 810 3836, Fax.: +82 53 810 4627
E-mail address: tjko@yu.ac.kr
† Recommended by Editor Haedo Jeong

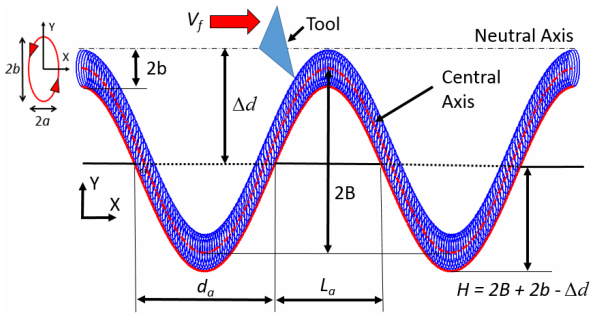

Fig. 1. Illustration of TFEVT method.

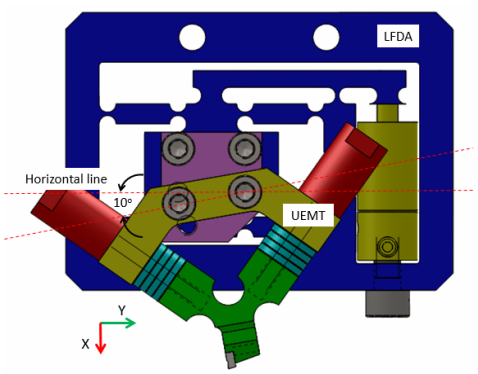

Fig. 2. Assembly of the TFEVT device.

the nominal relative cutting velocity, and t is time.

The elliptical motion has minor and major amplitudes, a and b, respectively, and B is the amplitude of the sinusoidal wave at low frequency. In UEVC [9], to achieve intermittent cutting so that the tool tip separates from the workpiece in each cut cycle, the maximum ultrasonic vibration velocity must be higher than the nominal relative cutting velocity, V_f. This intermittent cutting requirement remains valid when the tool tip reaches the bottom of the micro-dimple.

$$\left(2\pi f_h \cdot a\right) > V_f \ . \tag{3}$$

A Double-frequency, elliptical vibration cutting (DFEVC) method was first proposed by Zhou et al. [10] for freeform surface profile generation in diamond turning. By applying low-frequency vibration of an elliptical locus at approximately 100 Hz and at a spindle rotational speed of 6 rpm, the free-form surface profile was created and the vibration marks were clearly observed [10]. In addition, Zhou et al. [11] developed a DFEVC apparatus in which the elliptical locus vibration frequency was generated at 100 Hz. The sinusoidal frequency was lower than 5 Hz. The apparatus operated at relatively low vibration frequencies of approximately 100 Hz. This apparatus might be suitable for profile generation of freeform surfaces in diamond turning. In contrast to Zhou's design, the TFEVT device operates in the ultrasonic frequency range (>20 kHz). A comprehensive study of surface roughness conducted using the TFEVT method has been published recently by Kurniawan et al. [12].

In this study, the design of a TFEVT device is proposed. The TFEVT device consists of two components: The UEMT and the LFDA. The UEMT operates in the ultrasonic frequency range (> 20 kHz) and generates two-dimensional motion in the tool tip. It operates at the 6th resonance normal vibration mode and the 6th resonance tangential vibration mode. The LFDA operates in frequency ranges lower than its 1st natural frequency, and generates relatively large amplitudes of sinusoidal motion. The performance of the two components was analyzed separately using analytical and experimental methods. Finally, the feasibility of the TFEVT method for a surface texturing process was determined using experimental assessments. Based on the experiments, the TFEVT method showed improved micro-groove surface roughness quality compared to the CT method.

2. Design of TFEVT device

In the TFEVT design, the UEMT is fixed at 10^o with respect to the horizontal line, as shown in Fig. 2. This positioning is required to increase the nominal clearance angle (≈17^o) to avoid contact between the flank face of the cutting tool and the machined surface during the surface texturing process. This arrangement causes the rake angle to become slightly negative (≈-3^o).

2.1 UEMT design

The UEMT design presented in this study was inspired by Guo's transducer design [13], which in turn adopted Kurosawa's ultrasonic motor conceptual design [14]. A transducer design based on this idea could produce considerably high mechanical power. Kurosawa's transducer was developed specifically for ultrasonic motor applications; thus, maximal output speed, force, and mechanical power were prioritized during the design process [14]. The novelty of the UEMT design is that the output amplitude of the elliptical locus was designed carefully to be less than 1 μm and the working frequency is approximately 24 kHz.

The UEMT design consists of two bolt-clamped Langevin transducers. Langevin transducers were chosen since they work ultrasonically (> 20 kHz). Each transducer incorporates four O-ring shaped piezoelectric actuators (PZT). Each PZT has a 15 mm outer diameter, 6 mm inner diameter, and is 2 mm thick. The piezo-crystal material is type S-44 and is produced by SunnyTec. Detailed material properties of the PZT are shown in Table 1.

The Computer aided design (CAD) model of the UEMT design is shown in Fig. 3. Each Langevin transducer is connected at the end of the 90^o tool holder (flexure hinge structure). The angle between the two Langevin transducers is set to 90^o, following Kurosawa's design [14]. The two end masses on both ends of the transducer provide a preload to the piezoelectric actuators. The length of the end mass was designed to be approximately 25 mm, and the diameter is similar

Table 1. Piezoelectric actuator, S-44 specification.

ρ g/cm^3	T_c °C	ε_{33}^T	tg δ	Q_m	d_{33} M/V	g_{33} Vm/N	E MPa
7.7	300	1550	0.4	1400	330x10^{-12}	23.4x10^{-3}	80000

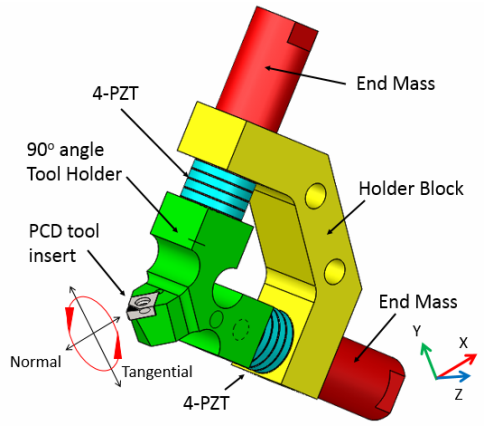

Fig. 3. CAD model of the UEMT design [13].

to the O-ring PZT diameter, approximately 15 mm. The 90° tool holder is composed of aluminum to provide a light weight or load to the PZT so that its optimum amplitude vibration could be achieved. The end mass material is medium alloy steel (AISI 1045). The holder block is considered to be a nodal point of the Langevin transducer, where the vibration due to resonance does not occur at the fixed nodal point.

Two main vibration modes are considered for the UEMT: Symmetrical (normal direction) and asymmetrical (tangential direction). The symmetrical mode shape occurs when the longitudinal direction of the Langevin transducer is in the in-phase condition. The asymmetrical mode shape occurs when the longitudinal direction of the Langevin transducer is in the out-of-phase condition. The symmetrical and asymmetrical mode shapes must have a similar natural frequency in order to vibrate the tool tip simultaneously in two directions.

A modal simulation was performed to predict the dynamic characteristics of the UEMT device (natural frequency and mode shape were of particular importance). ANSYS commercial software was used to identify the natural frequencies of each of the symmetrical and asymmetrical mode shapes. Table 2 shows the modal simulation results for three different end mass lengths (20, 25 and 30 mm). The natural frequency of each mode depends on the length of the end mass [13]. By increasing the length of the mass, the natural frequency of each mode reduces. Since the desired working frequency of the UEMT design is approximately 30 kHz, the 25 mm end mass length was used in the current design. Based on the modal simulation results, the 4th symmetrical and 4th asymmetrical mode shapes have similar natural frequencies: 30.67 and 30.5 kHz, respectively. Figs. 4(a) and (b) show the symmetrical and asymmetrical 4th mode shapes, respectively.

In a previous study, Shi et al. [15] proposed a mathematical

Table 2. Modal simulation analysis of the UEMT design.

	End mass: 20 mm		End mass: 25 mm		End mass: 30 mm	
Nth	Symmetric (Hz)	Asymmetric (Hz)	Symmetric (Hz)	Asymmetric (Hz)	Symmetric (Hz)	Asymmetric (Hz)
1st	9487	11833	8066.9	10348	6674.9	8969.3
2nd	14653	20327	12722	18623	11853	17797
3rd	24918	27897	24537	27686	24496	27710
4th	**31738**	**31852**	**30677**	**30501**	**28743**	**29509**
5th	37649	43342	35225	42174	33400	37234

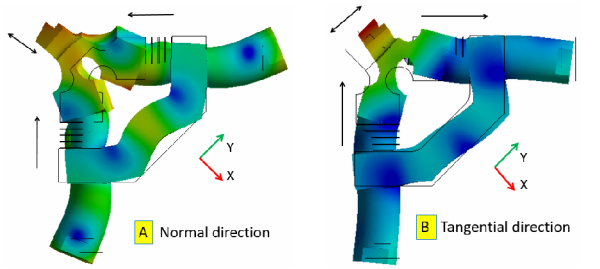

(a) (b)

Fig. 4. UEMT mode shapes: (a) 4th symmetrical mode shape; (b) 4th asymmetrical mode shape.

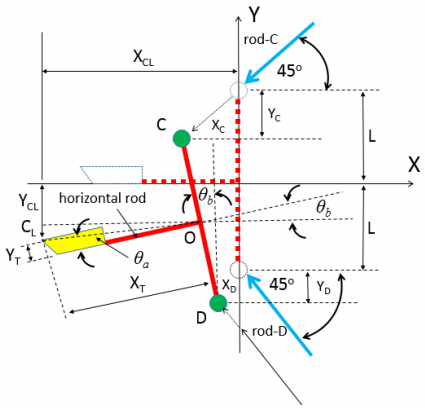

Fig. 5. Kinematic analysis of the UEMT design [15].

model to analyze the trajectory of the tool tip when it vibrates in two dimensions. A schematic of the kinematical model is shown in Fig. 5. The 90° tool holder (flexure hinge structure) is simplified as a T-shaped bar. Points C and D indicate where the independent PZT pushes the T-shaped bar. The PZTs that push in the longitudinal direction are called rod-C and rod-D. The angle between the two Langevin transducers was set to 90°. In the schematic, the angle between rod-C and rod-D is set to 90°. In the equations described below, the amplitudes generated by each PZT are defined as C and D, f is the frequency of vibration, ϕ is the phase shift, and t is time. The displacement generated by each PZT actuator in the x (normal) and y (tangential) directions can be described as follows:

$$X_C = -C \cdot \sin(2\pi f \cdot t) \cdot \cos(45^o) \quad (4)$$

$$X_D = -D \cdot \sin\left(2\pi f \cdot t + \phi\right) \cdot \cos\left(45^o\right) \tag{5}$$

$$Y_C = L - C \cdot \sin\left(2\pi f \cdot t\right) \cdot \sin\left(45^o\right) \tag{6}$$

$$Y_D = -\left(L + D \cdot \sin\left(2\pi f \cdot t + \phi\right) \cdot \sin\left(45^o\right)\right). \tag{7}$$

X_C and X_D are the sinusoidal displacements of the rod-C and rod-D PZT actuators, respectively, along the *x*-axis. Y_C and Y_D are the sinusoidal displacements of rod-C and rod-D, respectively, along the *y*-axis. L is half of the total length between points C and D.

Fig. 5 shows the condition when the T-shaped bar is pushed by PZT actuators in both longitudinal directions. C_L is the cutter location of the tool tip, where the initial position is located at (X_T,Y_T) in the Cartesian (x,y) coordinate system. C_L refers to point O, in which O (0,0) is the center point of the T-shaped bar located between points C and D. θ_a is a constant angle of C_L, which refers to the O center point. θ_a can be calculated by Eq. (8).

$$\theta_a = \tan^{-1}\left(\frac{Y_T}{X_T}\right). \tag{8}$$

θ_b describes the angle between the horizontal rod of the T-shaped bar and the *x*-axis. θ_b can be described by Eq. (9).

$$\theta_b = \tan^{-1}\left(\frac{X_C - X_D}{\sqrt{\left(2L\right)^2 + \left(X_C - X_D\right)^2}}\right). \tag{9}$$

Point O (O_X, O_Y) can be formulated into Eqs. (10) and (11) because the T-shaped bar is symmetrical.

$$O_X = \frac{X_C + X_D}{2} \tag{10}$$

$$O_Y = \frac{Y_C + Y_D}{2}. \tag{11}$$

According to Fig. 5, when the T-shaped bar vibrates, the position of the cutter C_L can be formulated into Eqs. (12) and (13).

$$X_{CL} = O_X - \sqrt{X_T^{\,2} + Y_T^{\,2}} \cos\left(\theta_b - \theta_a\right) \tag{12}$$

$$Y_{CL} = O_Y - \sqrt{X_T^{\,2} + Y_T^{\,2}} \sin\left(\theta_b - \theta_a\right). \tag{13}$$

The final equation of C_L could be obtained by substituting Eqs. (10) and (11) into Eqs. (12) and (13), respectively. The final equations of the cutter location can be described as follows:

$$X_{CL} = \frac{-C \cdot \sin\left(2\pi f \cdot t\right) \cdot \cos\left(45^o\right) - D \cdot \sin\left(2\pi f \cdot t + \phi\right)\cos\left(45^o\right)}{2} - \sqrt{X_T^{\,2} + Y_T^{\,2}} \cos\left(\theta_b - \theta_a\right) \tag{14}$$

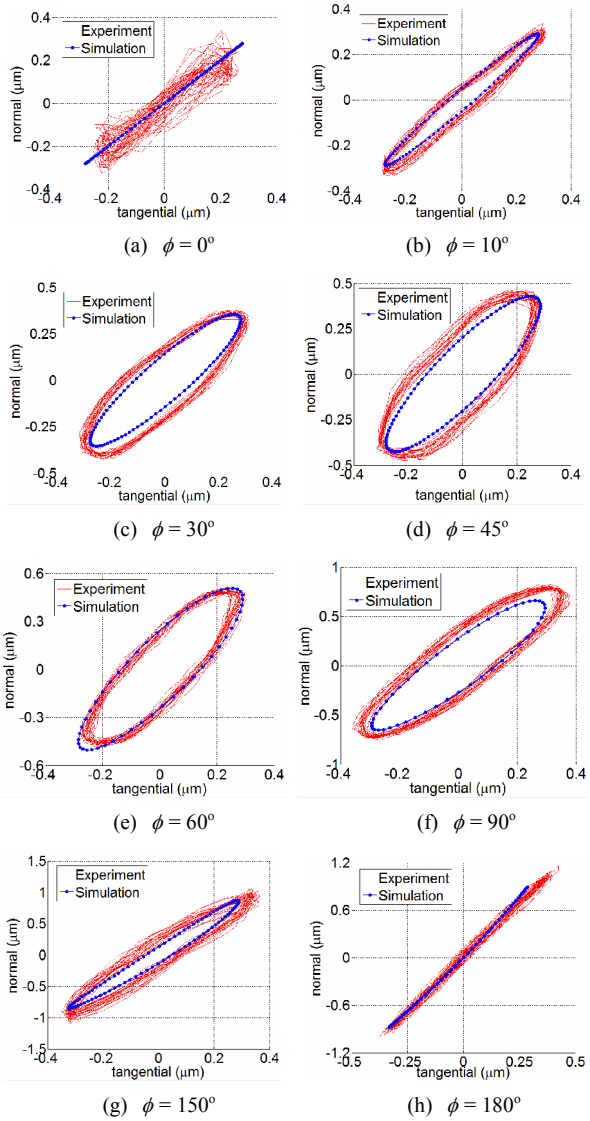

Fig. 6. Elliptical locus generated by the UEMT with different phase shifts.

$$Y_{CL} = \frac{-C \cdot \sin\left(2\pi f \cdot t\right) \cdot \sin\left(45^o\right) - D \cdot \sin\left(2\pi f \cdot t + \phi\right) \cdot \sin\left(45^o\right)}{2} - \sqrt{X_T^{\,2} + Y_T^{\,2}} \sin\left(\theta_b - \theta_a\right). \tag{15}$$

In case of amplitudes C and D, a generated amplitude of both PZT actuators can be estimated by using Eq. (16). N is the quantity of PZT actuators; d_{33} is the coefficient direction; and $V_{p\text{-}p}$ is the peak-to-peak voltage amplitude. Based on Table 1, the estimated amplitude of the PZT actuator is approximately 0.396 μm, where d_{33} = 330 x 10^{-6} μm/V, $V_{p\text{-}p}$ = 300 V and N = 4.

$$U = N \cdot d_{33} \cdot V_{p-p}. \tag{16}$$

C_L was simulated and the comparison with the measured results is presented in Fig. 6. It shows the trajectories of ellipti-

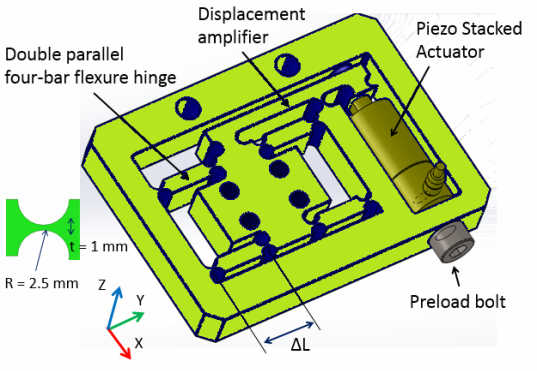

Fig. 7. Design of the LFDA.

cal loci that are generated by the UEMT with different phase shifts. The elliptical locus shape changes as the phase shift, ϕ, *r*anges from 0°-180°. A good agreement between the simulated displacement and the measurement has been achieved. The input parameters of the simulated displacement are similar to the input parameters when the two Langevin transducers were driven. During the measurement, the UEMT was driven at 24 kHz frequency with voltage input ($V_{p\text{-}p}$) of 300 V. The details of the dynamic characteristics of the UEMT are presented in Sec. 3. The UEMT generates a relatively small (< 1 μm) amplitude of elliptical locus, because the generated amplitude of the UEMT requires less than the generated amplitude of the LFDA.

2.2 LFDA design

The LFDA design was based on the non-resonance frequency mode and was carefully planned to have a longer displacement amplitude than the locus amplitude generated by the UEMT. The design was inspired by Lee's design [16, 17] for an atomic microscope application, in which a displacement amplifier was incorporated. The LFDA should have a sufficient displacement to cut the workpiece material, the displacement amplification ratio, r, was set to 5. The LFDA consists of the displacement amplifier, the double parallel four-bar flexure hinge structure, and the piezo stack actuator, as shown in Fig. 7. A flexure hinge mechanism was used because of the absence of friction. The piezo stack type P-212.10 actuator (manufacturer - Physik Instrumente) is used in this study. The piezo stack actuator is able to generate a maximum displacement of 15 μm and maximum force of 2000 N under the condition of no external load.

The estimation of the equivalent stiffness of the double-parallel four-bar flexure hinge is important for determining the displacement output generated by the LFDA in the *x*-direction. Based on Refs. [18, 19], the equivalent stiffness, K_{eqv}, is a function of the bending stiffness of the flexure hinge and the length between two flexure bars. Since the effect of the linear stiffness of the flexure bar, K_S, is relatively small in this case, the linear stiffness effect can be neglected. The estimation of K_{eqv} is presented in Eq. (17).

$$K_{eqv} = \frac{8K_B}{(\Delta L)^2} \tag{17}$$

where K_{eqv} is the equivalent stiffness, K_B is the bending stiffness, ΔL is the distance between two flexure bars measured from the center of the flexure hinge rotation. To estimate the value of K_B, Lobontiu [20] developed a precise equation, as shown in Eq. (18). In this equation, R is the radius of the flexure hinge, t is the thickness of the flexure hinge, w is the width of the flexure hinge, and E is the modulus of elasticity. K_B is the inverse of compliance of symmetric circular flexure hinge $C_{\theta,Z}$.

$$K_B = \frac{1}{C_{\theta,Z}}. \tag{18}$$

The compliance of the symmetric circular flexure hinge $C_{\theta,Z}$ is formulated as follows.

$$C_{\theta,Z} = \frac{24R}{Ewt^3(2R+t)(4R+t)^3}\left[t(4R+t)\left(6r^2+4Rt+t^2\right)\right. \\ \left.+6R(2R+t)^2\sqrt{t(4R+t)}\tan^{-1}\sqrt{1+\frac{4R}{t}}\right]. \tag{19}$$

K_{eqv} is approximately 2.63 N/μm, where t is 1 mm, R is 2.5 mm, w is 15 mm, E of AISI 1045 is approximately 205000 MPa, and ΔL is approximately 21 mm.

The estimation of the displacement output could be predicted using Eq. (20), based on the displacement output estimation of the atomic force microscope. Using the maximum force of the piezo actuator, 2000 N, and the maximum displacement, 15 μm, the estimated displacement output, x, was calculated to be approximately 8.947 μm. This was accomplished by neglecting the effect of external forces (cutting force). The preload displacement is approximately 125 μm, which was obtained by measurement using an optical displacement sensor when a preload force was given by a preload bolt.

$$x = \left(\frac{r\cdot x_{\max}\cdot F_{\max}}{F_{\max}+r^2\cdot K_{eqv}\cdot x_{\max}} - \frac{r^2\cdot x_{\max}\cdot K_{eqv}\cdot x_{preload}}{F_{\max}+r^2\cdot K_{eqv}\cdot x_{\max}}\right) - \left(\frac{F_{ext}}{K_{eqv}}\right) \tag{20}$$

where x_{max} is the maximum displacement output of the piezo actuator without a blocked force, F_{max} is the maximum force of the piezo actuator without a blocked force, K_{eqv} is the stiffness equivalent of the double parallel flexure hinge, r is the displacement amplifier ratio, and F_{ext} is the given external force. In general, F_{ext} is the cutting force during the surface texturing process, and it significantly affects the displacement output. In previous work [21], the maximum cutting force during the micro-dimpling process is approximately 2 N, and it can be predicted that the displacement output will reduce to

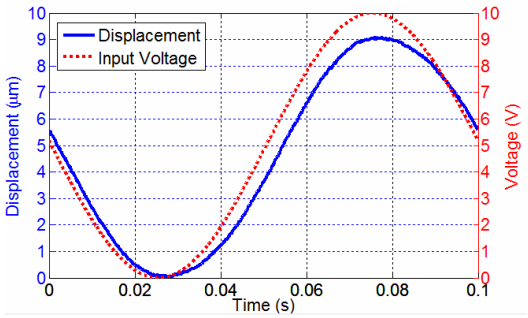

Fig. 8. Displacement output measurement of the LFDA at f_l 10 Hz.

approximately 8 μm. If a micro-groove pattern is established, it might increase the cutting resistance; thus the displacement output could be approximately 6-7 μm. Fig. 8 shows the measured results of displacement output when the piezo actuator was driven under a voltage input range of 0-1100 V with a vibration frequency f_l of 10 Hz, in which voltage input from the function generator was approximately 0-10 V. The displacement output between peaks is approximately 9 μm, which corresponds well with the 8.947 μm approximate prediction.

The generated force from the piezo actuator is presented in Eq. (21). The generated force was estimated to be approximately 117.5 N. This force is sufficient for the surface texturing process, because it requires cutting forces less than 5 N.

$$F_p = r \cdot K_{eqv} \cdot x \,. \tag{21}$$

3. Dynamic characteristic results

To investigate the dynamic characteristics of the TFEVT device, a Frequency response function (FRF) analysis was carried out. The excitation input signals are generated from a data acquisition device (NI DAQ USB-6251) manufactured by National Instruments. The output displacement was recorded using an optical displacement sensor, and then the output signal was sent back to the DAQ apparatus. In the UEMT case, the excitation voltages have a maximum peak of approximately 300 V, which is generated by an ultrasonic generator manufactured by Hybrid Precision. In the LFDA case, the excitation voltages have a maximum peak of approximately 1000 V, which is generated by an E.508 model linear amplifier (manufactured by Physik Instrumente). During the impact test experiment, which was only conducted for the LFDA, the FRF signal was analyzed up to 100 kHz by an HP digital signal analyzer and accelerometer (manufactured by B & K Instruments).

In the UEMT case, the FRF was performed by applying a sine sweep, in which sinusoidal excitation signals were applied with continuously varying frequencies. In this case, the frequency range was chosen to range from 100 Hz to 100 kHz. The two Langevin actuators were energized simultaneously by a sinusoidal signal in zero phase. The FRF function in the normal (*x*-direction) and tangential (*y*-direction) directions

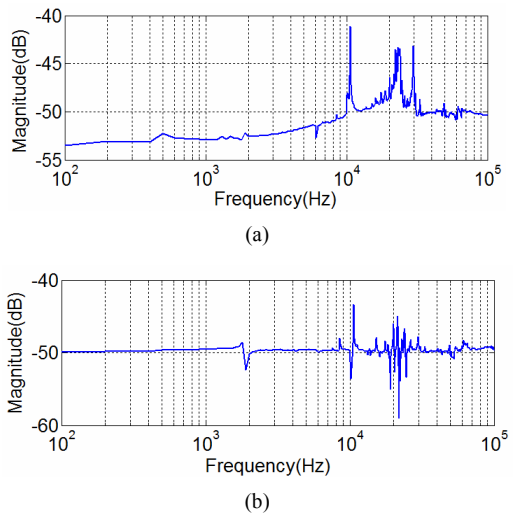

Fig. 9. UEMT FRF graphs for (a) the normal; (b) tangential directions (PCD tool attached).

were captured and investigated. Fig. 9 shows the captured UEMT FRF graphs for the normal and tangential directions where the effect of the PCD tool tip has been investigated. By adding a mass on the tip, such as the Polycrystalline diamond (PCD) tool or the Cubic boron nitride (CBN) tool, the natural frequency of the UEMT shifts slightly lower than its natural frequency without a tool tip installed. In the case without a tool tip installed, the results show that the 1st natural frequency occurs at 10.7 kHz for both the normal and tangential directions. The strongest magnitudes for the normal direction occur at the 1st, 4th and 6th natural frequencies, which correspond to values of 10.7 kHz, 24.1 kHz (approximate), and 31.1 kHz (approximate). In the 6th natural frequency, the normal direction is dominant and the tangential direction does not appear. When the PCD tool is installed, the natural frequency reduces slightly; the 1st natural frequency becomes 10.6 kHz. In addition, new natural frequency peaks appear in the range of 20-24 kHz (without tool). Based on the results in the case with the PCD tool installed, the similar frequencies for the normal and tangential directions are approximately 10.6 kHz for the 1st natural frequency, 24 kHz for the 6th, and 29.9 kHz for the 7th. In the case with the CBN tool installed, the similar frequencies for the normal and tangential directions are only 10.6 kHz for the 1st and 24 kHz for the 6th. A summary of the results from the FRF experiments is shown in Table 3.

In the LFDA case, the sine sweep was applied to identify the FRFs associated with the vibration behavior of the LFDA in the *x*-direction, under various vibration frequencies (1 Hz to 3 kHz). According to the FRF results in Fig. 10, the stable amplitude range is lower than approximately 400 Hz. Subsequently increasing the vibration frequencies greater than 400 Hz, the amplitude arbitrarily decreases and vibrates unsteadily. In addition, an impact test was conducted to analyze the natural frequency of each mode shape in the *x*, *y* and *z* directions. The results for the simulation and experiment are summarized in Table 4. Based on this table, the results from

Table 3. Summary of UEMT FRF results.

f_n^{th}	No tool tip		PCD tip		CBN tip	
	N	TG	N	TG	N	TG
1st	10.7	10.7	10.6	10.6	10.6	10.6
2nd	20.3	20.4	20.3	20.1	20.3	20.0
3rd	22.3	22.3	22.3	20.3	22.3	20.3
4th	24.1	24.4	22.9	21.5	22.9	21.5
5th	26.3	26.4	23.3	23.1	23.3	23.0
6th	31.1	-	24.0	24.0	24.0	24.0
7th	-	-	29.9	29.9	29.8	33.2

N = Normal; TG = Tangential; Unit = kHz

Table 4. LFDA modal simulation and experimental results.

	Simulation	Swept	Impact		
f_n^{th}	Resultant (Hz)	x-dir (Hz)	x-dir (Hz)	y-dir (Hz)	z-dir (Hz)
1	1179	1060	1072	1072	-
2	1316.5	-	1200	1200	1200
3	2198.6	1777	2136	2136	-
4	2427.7	-	2320	2320	2320
5	3094.2	2909	2920	2920	-

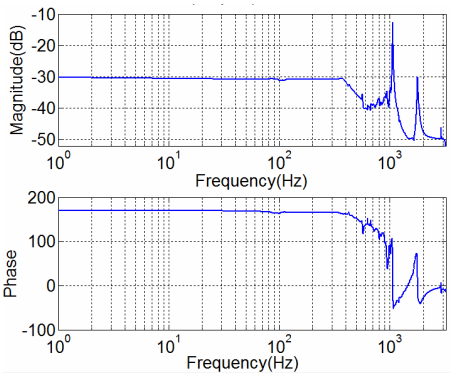

Fig. 10. FRF of the LFDA swept sine experiment.

the modal simulation and the actual experiment (sine sweep and impact) are in good agreement. Based on the impact test results, the 1st mode shape occurs when the double parallel flexure structure moves in the *x*-direction; the natural frequency value is approximately 1072 Hz. The natural frequency of the 1st mode shape is useful for amplification displacement, while the structure vibrates in a resonance condition in the *x*-direction. However, the working frequencies of LFDA are maintained lower than the natural frequency of the 1st mode shape. It can be understood that during resonance, the vibration and amplitude are not stable, which may affect the textured surface results.

4. Preliminary surface texturing results

The TFEVT device was used to conduct preliminary surface texturing assessments to investigate the feasibility of the device for use in such a process. The trial setup is shown in Table 5, where the sinusoidal micro-groove pattern was established on an AISI 1045 steel (H_RC = 30). A PCD tool was used during the micro-grooving process, in which a nominal rake angle of -3° and a nominal clearance angle of 17° were set. To establish a planar surface, where the nominal depth of cut (*H*) is identical for each micro-groove, a pre-machining process using a milling method was performed first using a 50 mm/min feed rate and a 12000 rpm rotational speed. Then, the distance between the tool tip and the workpiece surface was adjusted.

Table 5. Preliminary sinusoidal micro-groove process.

Texturing parameters	**CT** method	**TFEVT** method
Low vibration frequency (f_l)	0, 10, 30, 50 Hz	0, 10, 30, 50 Hz
Ultrasonic vibration frequency (f_h)	-	24 kHz
Phase shift (ϕ)	-	90°
Nominal cutting velocity (V_f)	500 mm/min	500 mm/min
Nominal depth of cut (H)	7 µm	7 µm
Δd	-10 µm	-10 µm
Cross-feed distance (F)	400 µm	400 µm
Minor amplitude (a)	-	0.3 µm
Major amplitude (b)	-	0.8 µm
Low vibration amplitude, B	4 µm	4 µm

In this case, the elliptical locus was generated at a constant working frequency of 24 kHz, and the phase shift was set at a constant 90°. Low vibration frequencies (f_l) of 10, 30 and 50 Hz were applied to investigate the effects of the elliptical motion of the tool tip. The cross-feed distance (F) is the distance between two sinusoidal micro-grooves and was set to a constant 400 µm. The nominal relative cutting velocity (V_f) was set to a constant value of 500 mm/min. The peak-to-peak amplitude of the sinusoidal wave ($2B$) was set to a maximum value of 8 µm (approximate). Then, to analyze the performance of the TFEVT method, a CT method with similar texturing conditions was performed as a comparison. The micro-groove pattern results were then captured by a 3D optical surface profiler, based on the White light scanning interferometry (WSI) principle, which was then used to analyze the 3D surface topography of the micro-groove results on the planar surface.

The experimental results for the micro-groove pattern are shown in Fig. 11. Fig. 11 only shows a comparison between the CT and TFEVT methods, in which the micro-groove pattern was established using low vibration frequencies (f_l) of 0 and 30 Hz. f_l = 0 Hz means that the sinusoidal wave was not applied. Based on Fig. 11(a), a side burr was generated in the micro-groove during the continuous cutting process. This may have been caused by high cutting resistance due to the size effect at the small nominal depth of cut on the side [22]. This can result in plastic side flow deformation, which produces burrs at cutting side regions. Meanwhile, the micro-groove morphology is better when the TFEVT method is applied. The

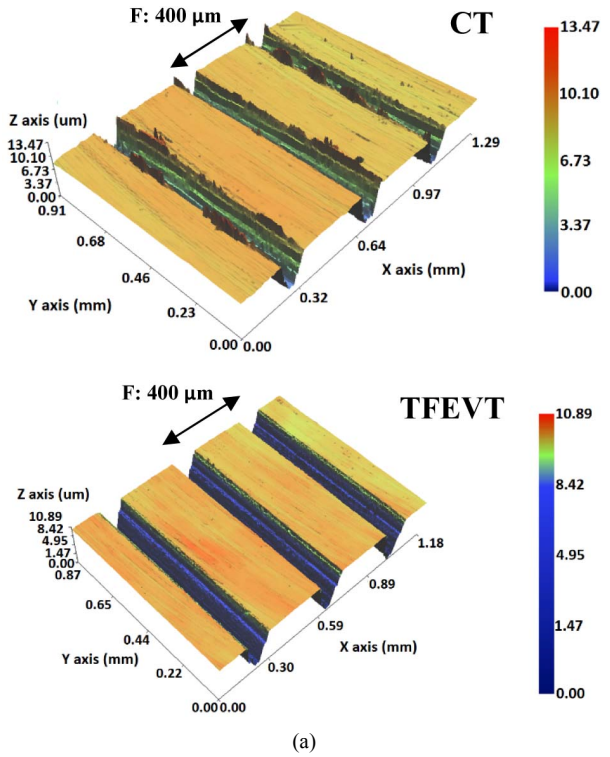

(a)

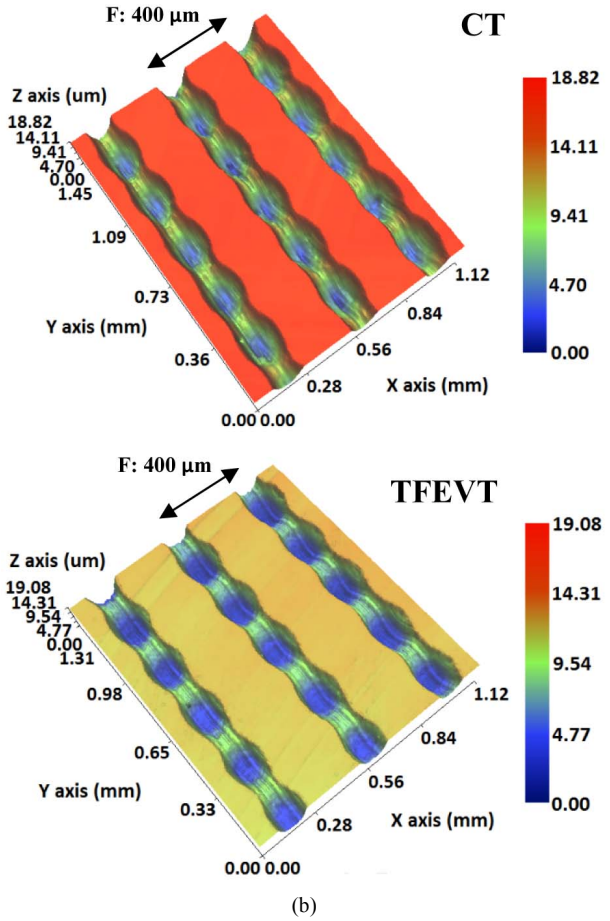

(b)

Fig. 11. Comparison of micro-groove pattern establish using CT and TFEVT methods: (a) f_l = 0 Hz; (b) f_l = 30 Hz.

TFEVT method reduces the frictional force between the tool rake face and the chip contact due to its intermittent cutting behavior (the tool tip moves elliptically in the ultrasonic range), yielding a low specific cutting energy that reduces and removes the side burr on the micro-groove.

The low frequency sinusoidal f_l = 30 Hz shown in Fig. 11(b) illustrates the micro-groove pattern results using the CT and TFEVT methods. The quality of the micro-groove is better with the TFEVT method than the CT method. The surface roughness in particular showed a dramatic improvement. It can be understood that the rake angle varies during the sinusoidal micro-groove process when using the CT method. During climbing cutting, the rake angle approaches a negative value. Because the rake angle is a negative value, the machining performance is poor, which means the cutting resistance increases [23]. Another possible reason is that the relatively slow cutting velocity of the process (V_f = 500 mm/min) causes high cutting load resistance and yields poor surface roughness of the micro-groove. By using the TFEVT method, the tool tip moves ultrasonically and the relative cutting speed is increased. Thus, the roughness of the micro-groove applied with the TFEVT method is reduced in comparison to the CT method.

5. Conclusion

In conclusion, in this study, a TFEVT device is proposed for surface texturing. Compared to previous TFEVT apparatuses, the novelty of the proposed TFEVT device is that it operates in the ultrasonic frequency greater than 20 kHz and the stable amplitude of low frequency vibration (f_l) has a large range of approximately 400 Hz. The TFEVT device consists of two components, the UEMT and the LFDA, and their dynamic characteristics were evaluated separately. The experimental results show that the UEMT operates at the 6th resonance vibration mode of the normal direction and at the 6th resonance vibration mode of the tangential direction at 24 kHz. The UEMT can generate elliptical loci at small amplitudes less than 1 µm. The LFDA operates in frequency ranges lower than its 1st natural frequency, and generates relatively large and stable sinusoidal wave amplitudes (approximately 9 µm) at frequencies lower than approximately 400 Hz. Finally, several experimental assessments of micro-groove patterns were conducted to evaluate the performance of the developed TFEVT device. Based on the experimental results, it is evident that the developed TFEVT device is suitable for improving the surface texturing quality on a carbon steel surface using a diamond cutting tool.

Acknowledgment

This research was supported by Basic Science Research Program through the National Research Foundation of Korea (NRF) funded by the Ministry of Science, ICT and future Planning (grant number NRF-2017R1A2B2003932). This

work was also supported by the Technology Innovation Program (grant number 10053248, Development of Manufacturing System for CFRP (Carbon Fiber Reinforced Plastics Machining) funded by the Ministry of Trade, Industry & Energy (MOTIE, Korea).

References

[1] A. Greco, S. Raphaelson, K. Ehmann and Q. J. Wang, Surface texturing of tribological vibromechanical texturing, *J. Manuf. Sci. Eng*., 131 (2009) 1-8.

[2] R. Kurniawan and T. J. Ko, A study of surface texturing using piezoelectric tool holder actuator on conventional CNC turning, *Int. J. Precis. Eng. Manuf*., 14 (2013) 199-206.

[3] E. Shamoto and T. Moriwaki, Ultaprecision diamond cutting of hardened steel by applying elliptical vibration cutting, *CIRP Ann. Technol*., 48 (1999) 441-444.

[4] G. D. Kim and B. G. Loh, Characteristics of chip formation in micro V-grooving using elliptical vibration cutting, *J. Micromechanics Microengineering,* 17 (2007) 1458-1466.

[5] E. Shamoto, N. Suzuki, T. Moriwaki and Y. Naoi, Development of ultrasonic elliptical vibration controller for elliptical vibration cutting, *CIRP Ann. - Manuf. Technol*., 51 (2002) 327-330.

[6] C. Nath, M. Rahman and K. S. Neo, A study on ultrasonic elliptical vibration cutting of tungsten carbide, *J. Mater. Process. Technol*., 209 (2009) 4459-4464.

[7] G. D. Kim and B. G. Loh, An ultrasonic elliptical vibration cutting device for micro V-groove machining: Kinematical analysis and micro V-groove machining characteristics, *J. Mater. Process. Technol*., 190 (2007) 181-188.

[8] T. Moriwaki and E. Shamoto, Ultrasonic elliptical vibration cutting, *CIRP Ann. - Manuf. Technol*., 44 (1995) 31-34.

[9] E. Shamoto and T. Moriwaki, Study on elliptical vibration cutting, *CIRP Ann. - Manuf. Technol*., 43 (1994) 35-38.

[10] X. Zhou, C. Zuo, Q. Liu and J. Lin, Surface generation of freeform surfaces in diamond turning by applying double-frequency elliptical vibration cutting, *Int. J. Mach. Tools Manuf*., 104 (2016) 45-57.

[11] X. Zhou, C. Zuo, Q. Liu, R. Wang and J. Lin, Development of a double-frequency elliptical vibration cutting apparatus for freeform surface diamond machining, *Int. J. Adv. Manuf. Technol*. (2016).

[12] R. Kurniawan, G. Kiswanto and T. J. Ko, Surface roughness of two-frequency elliptical vibration texturing (TFEVT) method for micro-dimple pattern process, *Int. J. Mach. Tools Manuf*., 116 (2017) 77-95.

[13] P. Guo and K. F. Ehmann, Development of a tertiary motion generator for elliptical vibration texturing, *Precis. Eng*., 37 (2013) 364-371.

[14] M. K. Kurosawa, O. Kodaira, Y. Tsuchitoi and T. Higuchi, Transducer for high speed and large thrust ultrasonic linear motor using two sandwich-type vibrators, *IEEE Trans. Ultrason. Ferroelectr. Freq. Control,* 45 (1998) 1188-1195.

[15] G. Shi, C. Zhang and Y. Li, The finite element analysis and optimization of an elliptical vibration assisted cutting device, *J. Appl. Mech. Eng*., 4 (2015).

[16] D.-Y. Lee, D.-M. Kim, D.-G. Gweon and J. Park, A calibrated atomic force microscope using an orthogonal scanner and a calibrated laser interferometer, *Appl. Surf. Sci*., 253 (2007) 3945-3951.

[17] H. P. Syahputra, T. J. Ko and B. M. Chung, Development of 2-axis hybrid positioning system for precision contouring on micro-milling operation, *J. Mech. Sci. Technol*., 28 (2014) 691-697.

[18] A. Woronko, J. Huang and Y. Altintas, Piezoelectric tool actuator for precision machining on conventional CNC turning centers, *Precis. Eng*., 27 (2003) 335-345.

[19] J. Shen, Analysis on the displacement performances of parallel four-bar flexure hinge mechanism, *ICEMI 2009 - Proc. 9th Int. Conf. Electron. Meas. Instruments* (2009) 4598-4601.

[20] N. Lobontiu, *Compliant mechanisms: Design of flexure hinges*, CRC Press (2002).

[21] R. Kurniawan, G. Kiswanto and T. J. Ko, Micro-dimple pattern process and orthogonal cutting force analysis of elliptical vibration texturing, *Int. J. Mach. Tools Manuf*., 106 (2016) 127-140.

[22] Y. Qiu, M. Gu and Z. Wei, Machining mechanism research of glass by discrete element method, *J. Mech. Sci. Technol*., 29 (2015) 1283-1288.

[23] M. Günay, I. Korkut, E. Aslan and U. Şeker, Experimental investigation of the effect of cutting tool rake angle on main cutting force, *J. Mater. Process. Technol*., 166 (2005) 44-49.

Rendi Kurniawan is currently a post-doctoral fellow in Yeungnam University, South Korea. He received B.Eng. degree from Universitas Indonesia, Indonesia. His M.S. Eng. degree in mechanical engineering was acknowledged from Yeungnam University, South Korea. He received Ph.D. degree in mechanical engineering from Yeungnam University, South Korea. His research interests are surface texturing, tribology, friction reduction, micro-dimple fabrication, and elliptical vibration texturing.

Tae Jo Ko is a Professor of mechanical engineering at Yeungnam University, South Korea. He received bachelor and master degrees from Pusan National Univestiry, South Korea. He received Ph.D. in mechanical engineering from POSTECH, South Korea. His research interests include development of machine tools, micro-cutting process, non-traditional machining, surface texturing using grinding, bio-machining, hybrid EDM-milling process, textured surface on cutting tools and deburring process of CFRP composite.